Short communication

Graphite/graphene oxide composite as high capacity and binder-free anode material for lithium ion batteries

Jingxian Zhang [a,b], Huaqiang Cao [c], Xiaolin Tang [a,b], Weifeng Fan [a], Gongchang Peng [a], Meizhen Qu [a,*]

[a] Chengdu Institute of Organic Chemistry, Chinese Academy of Sciences, Chengdu 610041, PR China
[b] University of Chinese Academy of Sciences, Beijing 100039, PR China
[c] Department of Chemistry, Tsinghua University, Beijing 100084, PR China

HIGHLIGHTS

- Graphite/graphene oxide composite is prepared for high capacity and binder-free anode.
- The reversible capacity of this composite exceeds 690 mA h g^{-1} at 0.5 C.
- The composite exhibits excellent cycle performance and rate capability.

GRAPHICAL ABSTRACT
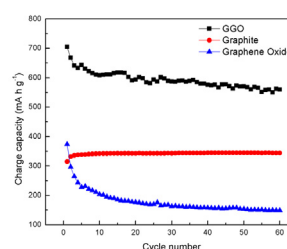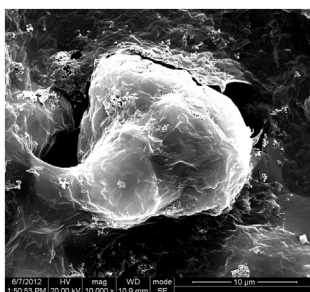
ABSTRACT

A composite of graphite and graphene oxide is synthesized and used as a high capacity and binder-free anode material directly in lithium-ion batteries for the first time. The scanning and transmission electron microscope analyses of the composite show the graphite particles and conductive additive are homogeneously distributed on the graphene oxide surface. The X-ray photoelectron spectroscopy result indicates that the oxygen containing groups of graphene oxide have been partially reduced during the first discharge process. Electrochemical tests reveal that this composite has more than 690 mA h g^{-1} reversible capacity at the rate of 0.5 C (1 C = 372 mA g^{-1}), simultaneously with excellent cycle performance and rate capability.

© 2013 Elsevier B.V. All rights reserved.

1. Introduction

Since the lithium-ion batteries (LIBs) were commercialized by the Sony Company in the early 1990s, carbon-based materials have been extensively used as anode materials in LIBs owing to their unique physical and electrochemical properties, although they revealed a low theoretical Li-ion storage capacity (372 mA h g^{-1}) [1]. Ongoing research efforts have focused on utilizing various new carbonaceous materials to improve the Li-ion storage capacity as well as cycle life and rate capability.

Graphene, a monolayer of carbon atoms, is often manufactured by reducing graphene oxide [2], has attracted significant attention

recently [3]. Due to its unusual properties such as high surface area to volume ratio, extraordinary electronic transport property and chemical stability [4], graphene holds many promising applications. One of the exciting possibilities is the application of graphene used as LIBs electrode materials. The studies of graphene-containing electrode materials, such as graphene modified $LiFePO_4$ cathode materials [5], graphene composites with nanosize alloys or transition metal oxides [6–8], and silicon nanoparticles—graphene paper composites [9], were explored by many researchers. And the Li-ion storage configuration of graphene proposed as anode material was not to be the conventional LiC_6, but the new LiC_3 [7], Li_2C_6 [10] or LiC_2 [11], which indicated a Li-ion storage capacity of 744, ~780 and ~1116 mA h g^{-1} respectively. Therefore, graphene is suggested to be an ideal candidate to replace graphitic carbon as the commercial anode material.

As the precursor of graphene, graphene oxide also has a higher lithium storage capacity than graphite [12,13] and performs excellent chemical stability and dispersity in water [14]. Besides, the preparation of graphene oxide is simple and feasible, and its cost is lower than graphene itself because it does not need a reduction treatment. However, graphene oxide is still on the periphery of attention, and the reports about its direct use as anode material in LIBs are hardly viewed.

Recently, many graphene-based nanocomposites have been applied as anode materials in LIBs [15–18]. However, these nanocomposites are synthesized costly in the view of commerce applications. In order to find a cheap and simple method to synthesize novel graphene-based materials used as electrode in LIBs, we apply a composite of commercial graphite, carbon black and graphene oxide (termed as GCG). In this composite, graphite can play a great role in holding out aggregation of graphene oxide sheets, stabilizing electrochemical property and providing Li-ion storage capability. Furthermore, this composite could be directly used as electrode without adding any other binders, because graphene oxide is effortless to form self-assembly membrane after drying. As such, the specific weight capacity of the GCG electrode could be improved in comparison with conventional electrodes which are assembled from a mixture of polymer binder, conductive additive and active materials. Electrochemical tests indicate that this GCG electrode exhibits a relatively high capacity, excellent rate capability, and cycling stability, as anode material of LIBs. To the best of our knowledge, for the first time, this could provide a new indication of applying graphene oxide directly in LIBs.

2. Experimental

2.1. Preparation of graphene oxide and GCG composite

Graphene oxide was synthesized from high-purity natural flake graphite (about 200 meshes, Changsha Shenghua Research Institute, 99.999%) by the Hummers method [19]. And the colloidal dispersion of graphene oxide in deionized water at the concentration of 1 mg ml^{-1} was prepared with the aid of ultrasound (20 kHz ultrasound probe) treatment about 15 min to give a stable brown dispersion. Conductive additive used in the composite was Super-P carbon black (40 nm, 62 m^2 g^{-1}, TIMCAL Graphite & Carbon). The anode slurries of graphene oxide, GCG and graphite were prepared by mixing adequate deionized water with (a) graphene oxide and carbon black (in a graphene oxide/ carbon black weight ratio of 83:17), (b) graphite, graphene oxide and carbon black (in a graphite/graphene oxide/carbon black weight ratio of 66:17:17, nominated as GCG-17%), (c) graphite, CMC (carboxymethyl cellulose, Aldrich, and M.W. 90,000) and carbon black (in a graphite:CMC:carbon black weight ratio of

66:17:17) through vigorously stirring for 3 h, respectively. Electrodes were fabricated by coating all above three slurries on Cu foil and dried overnight at 110 °C. The above processes were repeated with variation of graphite/carbon black/graphene oxide weight ratio to 75:17:8 (GCG-8%), 71:17:12 (GCG-12%), 62:17:21 (GCG-21%) and 58:17:25 (GCG-25%).

2.2. Characterization

Scanning electron microscope (SEM) studies were performed using an INCA PentaFETx3 microscope equipped with energy dispersive X-ray spectroscopy detector (EDS, to determine the chemical composition). The thickness of graphene oxide film was determined by atomic force microscope (AFM, SPI4000). The morphology of the GCG was characterized by transmission electron microscope (TEM, JEM-100CX JEOL). The elemental compositions and the assignments of the carbon peaks were characterized using the X-ray photoelectron spectroscopy (XPS, PHI5600 Physical Electronics). X-ray diffraction (XRD) patterns were obtained from X'Pert MPD DY1219 using Cu/Kα radiation ($\lambda = 1.5406$ Å). The specific surface areas and porosimetries were calculated by using the Brunauer—Emmett—Teller (BET) and the Barrett—Joyner—Halenda (BJH) method based on the adsorption branches of isotherms. The results of nitrogen adsorption—desorption isotherms measurements are presented in Supplementary data.

2.3. Electrochemical measurements

Electrochemical measurements were performed at room temperature (25 °C) using two-electrode CR2032 coin cells assembled in an argon-filled glove box. A Celgard 2400 was employed as separator. Lithium foil was used as counter electrode. The electrolyte obtained from Capchem. Technology (Shenzhen) Co., Ltd. consisted of a solution of 1 M $LiPF_6$ in ethylene carbonate, dimethyl carbonate, diethyl carbonate (EC/DMC/DEC, 1:1:1, in volume). Galvanostatic charge and discharge experiments were conducted at various rates on a BS-9300R battery test system, over the potential range 0.01—3.0 V versus Li^+/Li. The cyclic voltammograms (CV) tests were performed on a LK9805 workstation.

3. Results and discussion

According to the TEM, SEM and AFM results of graphene oxide revealed in Fig. 1a—c, it is clear that the single layer graphene oxide (0.55 nm thickness) with typical wrinkled paper-like structure has been prepared successfully by Hummers methods. Fig. 1d shows the C1s XPS spectrum of graphene oxide. The four dominant peaks emerged at 284.6, 285.7, 286.7 and 288.2 eV correspond to C—C/C= C, C—N, C—O and C=O species, respectively [20,21]. The weak peak at 285.7 eV ascribes to a C—N species, which is resulted from the oxidation process. The peaks at 286.7 and 288.2 eV confirm the presence of hydroxyl, epoxy and carbonyl groups on the surfaces and edges of the graphene oxide sheets.

Microscopic observation results of the graphene oxide, GCG-17% and graphite electrodes are given in Fig. 2. Fig. 2a shows the microappearance of graphene oxide electrode, which has a typical two dimensional (2D) wrinkled paper-like structure. The sole carbon black particles are packaged by graphene oxide sheets and dispersed uniformly. And in Fig. 2b, there are only agglomerate carbon black and graphite particles conglutinated by CMC in graphite electrode. In comparison, as observed in Fig. 2c, the graphene oxide sheets wrapping graphite and carbon black particles can be vividly viewed in GCG-17% electrode. In this composite, the carbon black particles are homo-dispersed between the graphene oxide sheets and graphite particles, which are beneficial for
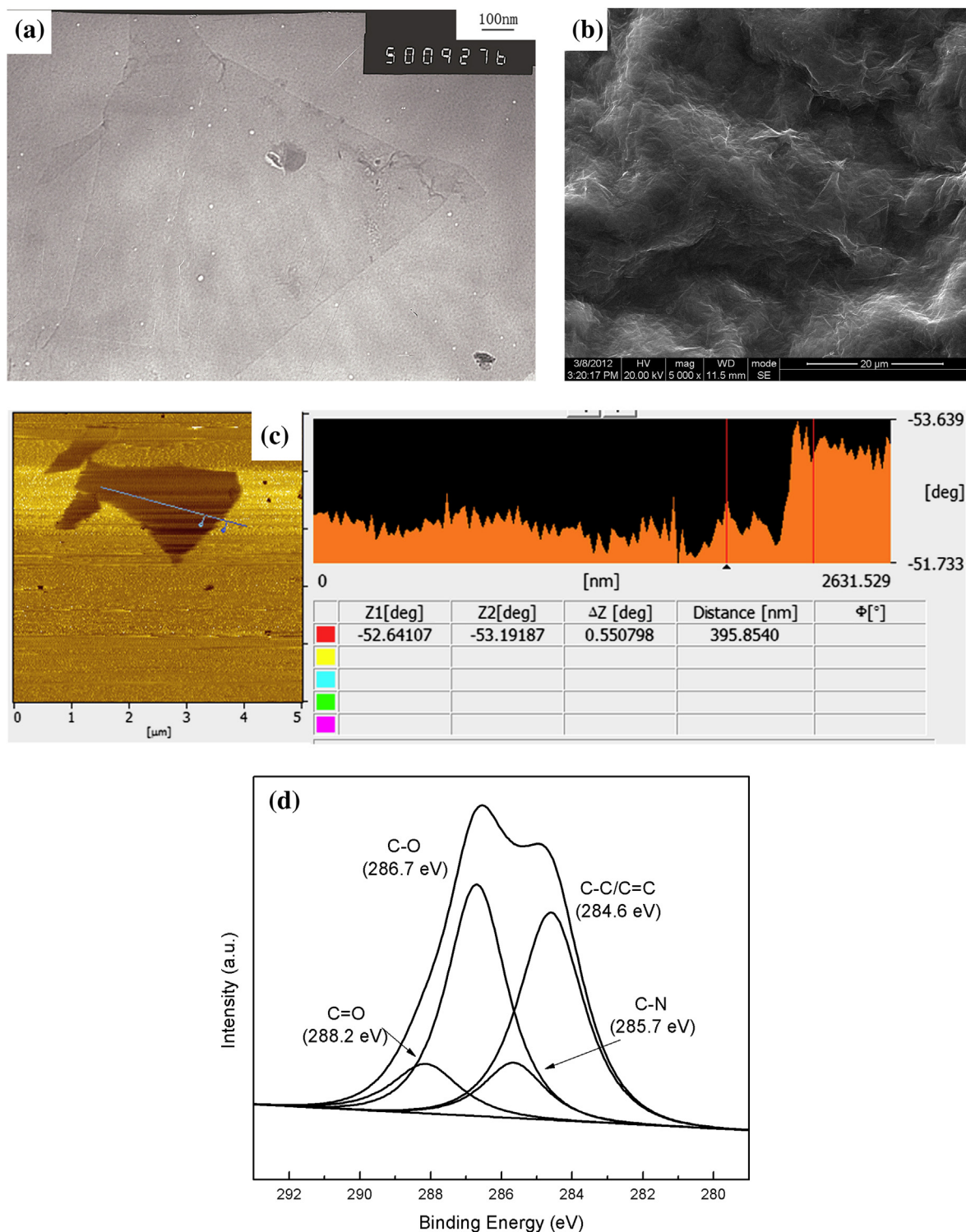
Fig. 1. Images of graphene oxide (a) TEM; (b) SEM; (c) AFM and (d) XPS.

enhancing the conductivity of the composite. The special morphology of this composite is also confirmed by TEM in Fig. 2d. As seen from Fig. 2d and its left inset, the carbon black particles attach well to the graphene oxide sheets and distribute equally, and the graphite particles are wrapped by graphene oxide entirely.

As shown in Fig. 3, the first discharge (Li-intercalation) and charge (Li-deintercalation) capacities of graphite, graphene oxide and GCG-17% electrodes at the rate of 0.5 C (1 C = 372 mA g^{-1}) are

compared. Graphene oxide shows the highest first discharge capacity (1388.3 mA h g^{-1}). However, this capacity is mostly irreversible and its first charge capacity is only 353.1 mA h g^{-1}. And the graphite electrode exhibits the first discharge and charge capacities of 370.2 and 314.5 mA h g^{-1}. Remarkably, GCG-17% electrode puts an amazing performance in both of the first discharge and charge capacities (1039.4 and 704.7 mA h g^{-1}), and this could be attributed to the Li$_2$C$_6$ [10] or LiC$_2$ [11] Li-ion storage configuration of
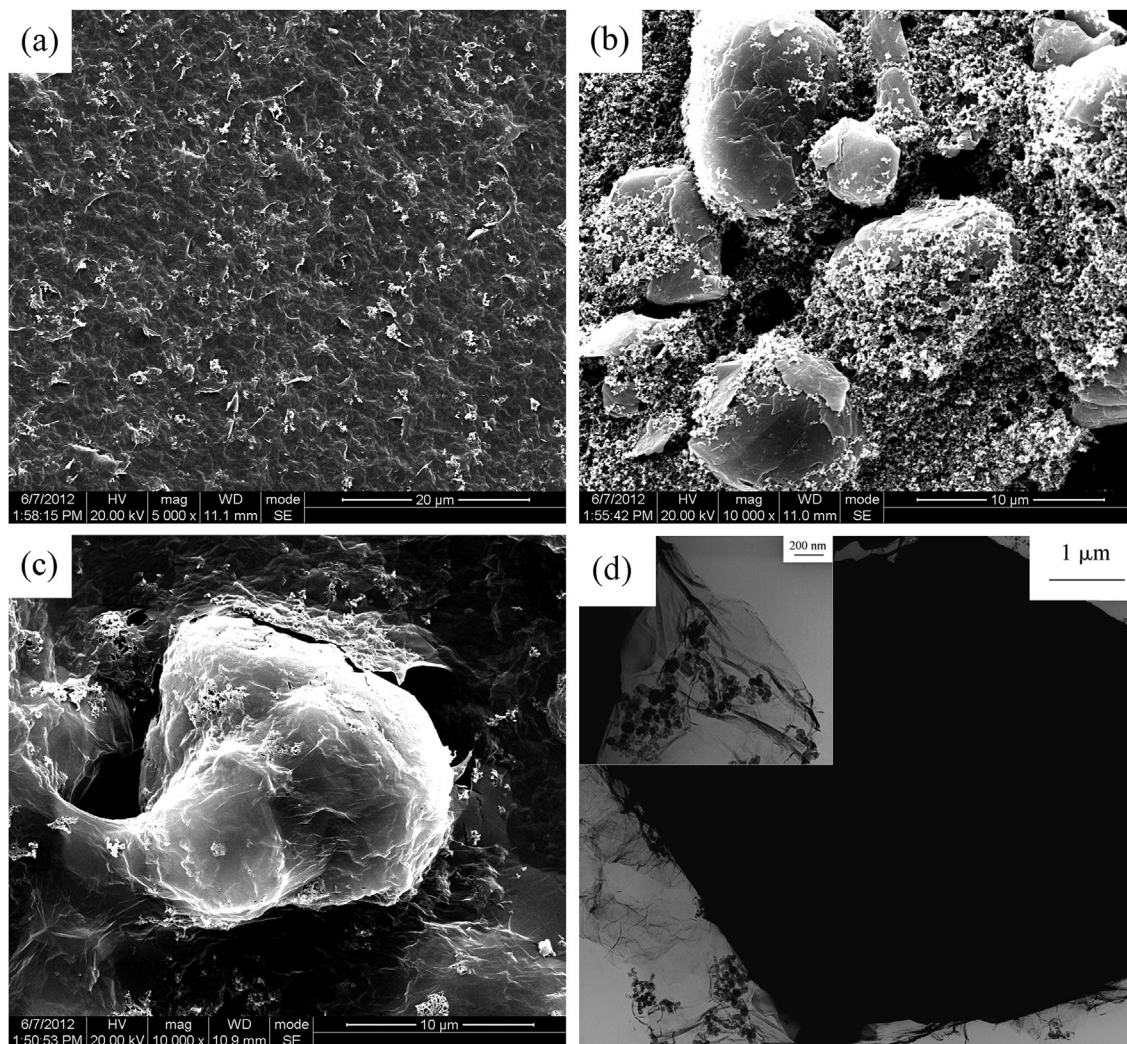
Fig. 2. SEM images of (a) graphene oxide, (b) graphite and (c) GCG-17% electrodes; (d) TEM image of GCG-17% electrode.
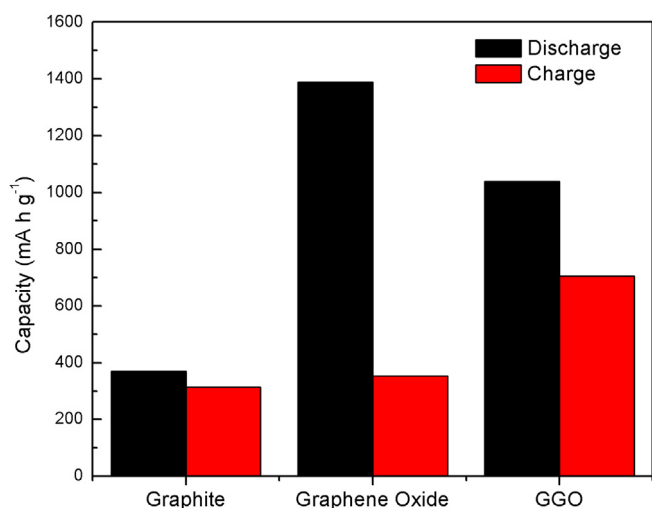

Fig. 3. First cycle discharge and charge capacity of graphite, graphene oxide and GCG-17% electrodes.

graphene as mentioned at the beginning. Moreover, the channels [22] and faradic capacitance [23] should also be taken into account. The GCG composite gives full play to the advantages of carbon black, graphite and graphene oxide. The graphite and carbon black improve the conductive ability while graphene oxide and graphite provide lithium storage capacity. Similar to most graphene-based LIBs electrodes, our graphene oxide and GCG electrode exhibited poor initial efficiencies (i.e., the % ratio of charge to discharge capacity) during the first cycle (25% and 68%, respectively) under the current rate of 0.5 C (Fig. 3). This is mainly originated from irreversible consumption of Li$^+$ which contains electrochemical reduction of surface functional groups [24,25] and forming solid-electrolyte interphase (SEI) film [7,26] (will be discussed later). However, it is anticipated that the graphene oxide could be employed for other active materials, such as MCMB, carbon nanotubes and silicon. Hence we can add or use some other materials with high Coulombic efficiency to attain a better coordination. Relative works are on the proceeding of our further work.

XPS measurement was employed to investigate the changes of the GCG-17% electrode before and after the discharge/charge process. Fig. 4 illustrates curve fitting of the C1s peak of XPS spectra. In Fig. 4a, four dominant peaks at 284.6, 285.7, 286.9 and 288.5 eV are respectively assigned to C–C, C–N, C–O and C=O species, respectively [20,21]. Compared with Fig. 4a, the C–N peak
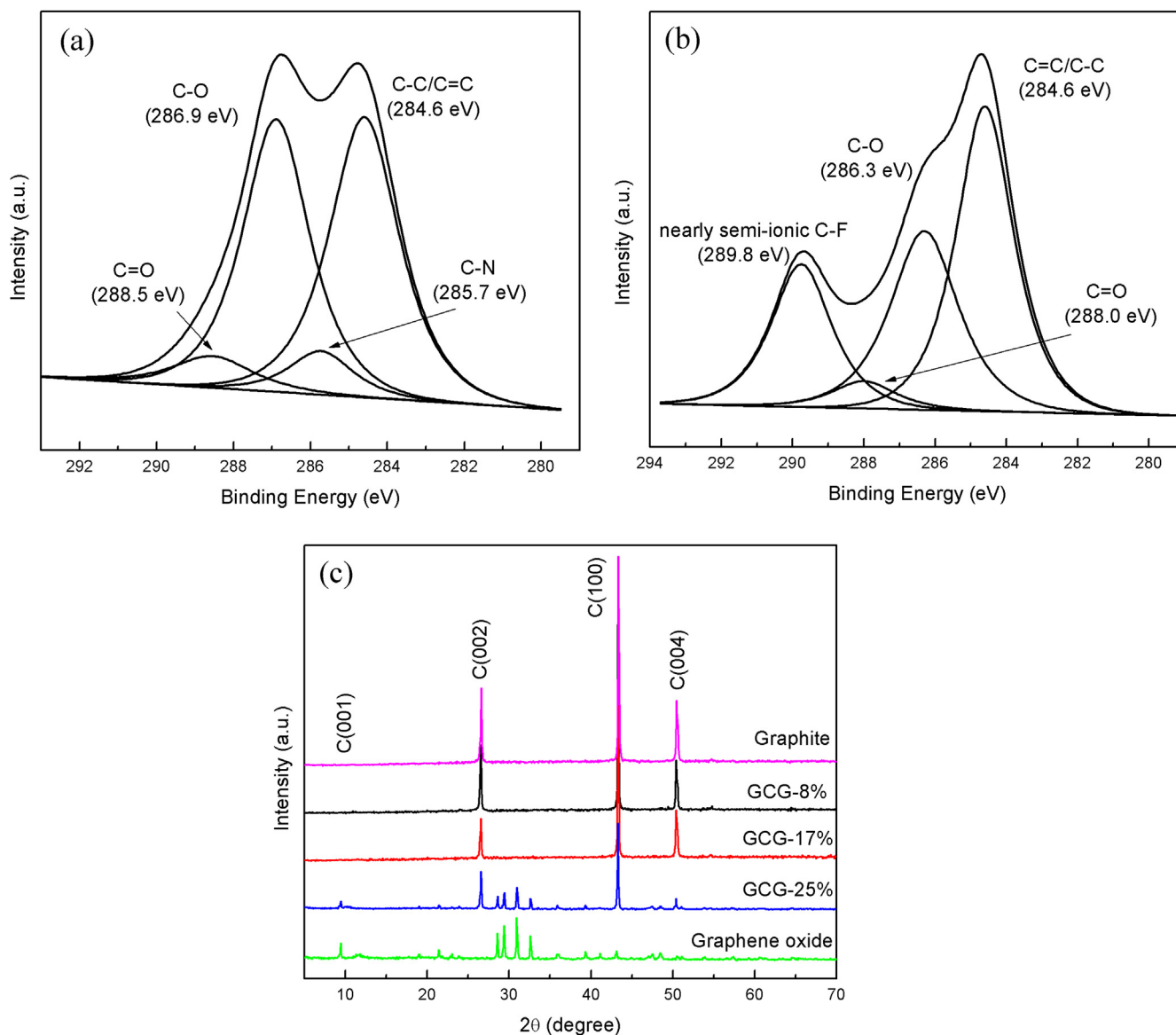
Fig. 4. C1s XPS of (a) GCG-17% electrode before electrochemical test and (b) GCG-17% electrode after the first discharge/charge cycle at the current rate of 0.1 C, (c) XRD patterns of graphite, GCG-8%, GCG-17%, GCG-25% and graphene oxide electrodes.

disappears and a new peak of nearly semi-ionic C–F [27] group arises in the Fig. 4b, and the peak of C–O shows a noticeable decrease and shifts slightly to lower binding energies, which signify the electrochemical reduction of part functional groups on graphene oxide sheet [28]. Similarly, as observed in Fig. 4b, the peak of C=O also shifts slightly to lower binding energies and the peak intensity presents some change.

XRD patterns of GCG-8%, GCG-17%, GCG-25% and graphene oxide electrodes are presented in Fig. 4c. The three GCG composites exhibit two characteristic peaks (002) and (100) of graphite at 26.54° and 43.34°, which are enhanced with the reduction of graphene oxide content. Simultaneously, an additional peak at 9.38° is disappeared and another strong peak at 50.48° is observed, which is corresponding to the (001) diffraction peak of graphene oxide [29] and (004) diffraction peak of graphite [30]. Notably, the ordered degree of GCG is partially recovered with the decrease of graphene oxide content, and such a change could affect the performance of lithium insertion of GCG electrode.

Nitrogen adsorption–desorption isotherms measurements were carried out for examining the specific surface area and pore volume

of GCG composites (Fig. S2a and b). The BET specific surface areas of GCG-8%, GCG-17% and GCG-25% are 11.95, 24.64 and 25.35 m^2 g^{-1}, respectively. The GCG composite has pores of sizes between 3.5 nm and 3.9 nm demonstrating a mesoporous structure, which is of benefit for increasing reversible lithium storage capacity.

Fig. 5a–c shows the first two potential profiles of the graphene oxide, graphite and GCG-17%/Li cell respectively, which were charged and discharged at a constant current rate of 0.5 C. From the first discharge curve in Fig. 5a, the capacity below 0.5 V could be primarily related to lithium intercalation into the graphene oxide sheets [4]. While, the capacity above 0.5 V may be ascribed to the faradic capacitance [23]. And some lithiation side reactions also occurred in both two processes, including the formation of SEI film [7,26] and reduction of trace water or surface groups [24,25]. For example, two slopes from 1.8 V to 1.0 V and from 1.0 V to 0.5 V nearly disappear in the second cycle. Besides, the slope from 0.5 V to 0.01 V in the second discharge curve is remarkably shorter than that in the first one, which suggests the possible aggregation of graphene oxide sheets or existence of defects [31]. Fig. 5b shows the typical discharge and charge curves of graphite. In the first discharge, the
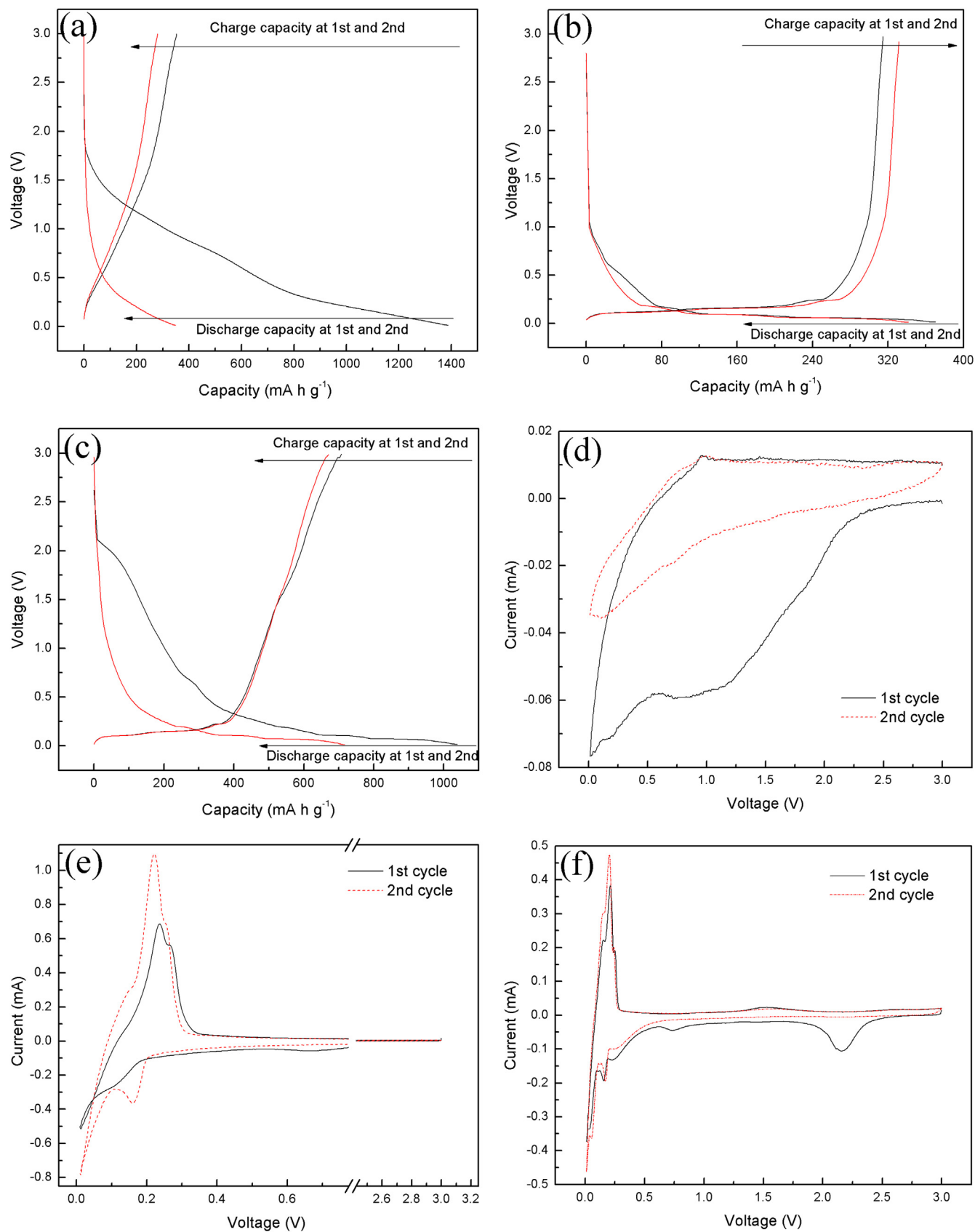
Fig. 5. The first and second charge/discharge profiles of the electrodes cycled between 0.01 V and 3 V (vs. Li$^+$/Li): (a) graphene oxide, (b) graphite, (c) GCG-17%, and relevant cyclic voltammograms of (d) graphene oxide, (e) graphite, (f) GCG-17% (scan rate: 0.1 mV s^{-1}).

slope from 0.8 V to 0.2 V is mainly attributed to the formation of the SEI film [32]. And the long plateau at ∼0.1 V is originated from the intercalation of lithium into graphite space. As shown in Fig. 5c, the first discharge curve of GCG-17% electrode presents characteristics of both graphene oxide and graphite electrodes. For instance, the curve of upper part is consistent with the voltage profile of graphene oxide, and the residual lower part matches well with that of graphite. Because both of graphene oxide and graphite have the ability of storing lithium, some slopes may overlap with each other. The first two charge/discharge profiles of GCG composites with different graphene oxide content are presented in Fig. S1a–f.

The cyclic voltammograms (CV) of graphene oxide, graphite and GCG-17% electrodes conducted at a scan rate of 0.1 mV s^{-1} from 0.01 V to 3.0 V vs. Li$^+$/Li are presented in Fig. 5d–f. In Fig. 5d, the reductive peak from 2.2 V to 0.5 V in the first cycle is corresponding to the formation of SEI film and reduction of trace water or surface groups [33], which vanishes away in the following cycle. Besides, the peak area from 0.5 V to 0.01 V in the first cycle is much large than that in the second one, indicating some fading of active sites. These peaks entirely show good correlations with the voltage profile (Fig. 5a). The CV (Fig. 5e) obtained from graphite electrode can be interpreted in detail from previous articles [32,34]. The

cathodic peaks observed at 0.19 V and 0.75 V in the first cycle of Fig. 5f can be ascribed to lithium intercalation into graphite layers [35] and formation of SEI film [24], respectively. And another broadened cathodic peak at 2.1 V may be attributed to the Li-intercalation into surface groups [36].

On the basis of cyclic performances of three electrodes at the current rate of 0.5 C (Fig. 6a), it is striking to note that a very high and stable reversible charge capacity of about 615 mA h g^{-1} in the initial 15 cycles (with a capacity loss per cycle of ∼1.20%), and 560 mA h g^{-1} after 60 cycles (with a capacity loss per cycle of ∼0.21%) are achieved for GCG-17% electrode. Although graphite electrode manifests the best cycling performance, its charge capacity is only ∼340 mA h g^{-1} after 60 cycles, far lower than that of GCG-17% electrode. As for graphene oxide electrode, after 60 cycles the reversible capacity decreases to 120.1 mA h g^{-1}, which is only 32.1% of its initial value (374 mA h g^{-1}). The capacity of GCG-17% electrode exceeds too much over the simple sum of that for graphene oxide and graphite electrodes.

To compare the rate capabilities of GCG-17%, graphite and graphene oxide electrodes, the capacity and stability at various current rates are tested and displayed in Fig. 6b. For GCG-17% electrode, an initial charge capacity of 695.3 mA h g^{-1} can be obtained for the GCG-
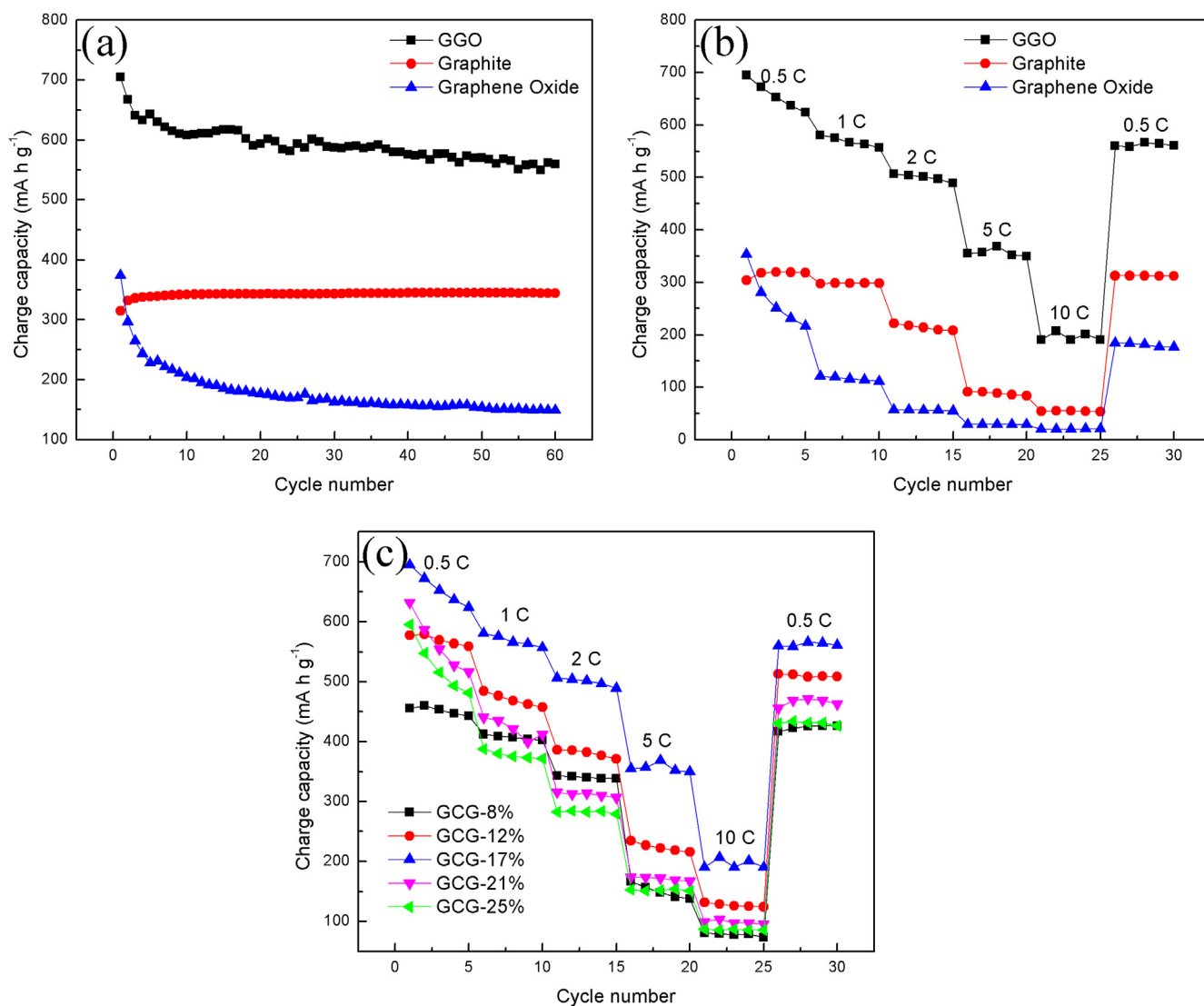

Fig. 6. (a) Cyclic performances of GCG-17%, graphite and graphene oxide electrodes; (b) rate capabilities of GCG-17%, graphite and graphene oxide electrodes at different rates; (c) rate capabilities of GCG-8%, GCG-12%, GCG-17%, GCG-21% and GCG-25% electrodes at different rates.

17% electrode at 0.5 C. Though this value shows some slight drops at 0.5 and 1 C, its capability is still better than that of other two electrodes, and a charge capacity of 190.2 mA h g^{-1} could be obtained even at the rate of 10 C. At the same rate, the charge capacities are only 52.7 and 20.7 mA h g^{-1} for graphite and graphene oxide electrodes, respectively. After cycling at various rates, when the current density comes back to 0.5 C, the capacity of GCG-17% electrode could return to its original value, suggesting a good reversity and steadiness.

In order to understand the effect of graphene oxide content on the reversible capacity and rate capability of the composite, five electrodes with different contents of graphene oxide (GCG-8%, GCG-12%, GCG-17%, GCG-21% and GCG-25%) are prepared and examined. As observed in Fig. 6c, the reversible capacity and rate capability of GCG electrode are varied with the content of graphene oxide, and it is obvious that both the reversible capacity and rate capability of GCG electrode will degrade with enhancing the weight ratio of graphene oxide or decreasing it. The GCG-17% electrode exhibits the relatively best performance.

4. Conclusions

A composite of GCG was synthesized by mixing the commercial graphite, graphene oxide and carbon black. After drying, a binder-free negative electrode was obtained. In this electrode, graphene oxide possesses both the functions of lithium storage and of a binder, and commercial graphite exerts an impact on both capacity and conductivity. Then carbon black dispersed uniformly between the graphene oxide sheets could also enhance the conductivity. So, the capacity, cyclability and rate capability of GCG electrode are visibly strengthened in comparison with those of graphene oxide and graphite electrodes. In this binder-free electrode, the GCG shows good adhesion to the substrate and more active materials are involved so as to attain a higher energy density.

Acknowledgements

Appendix A. Supplementary data

Supplementary data associated with this article can be found in the online version, at http://dx.doi.org/10.1016/j.jpowsour.2013.05.001.

References

[1] L. Ji, Z. Lin, M. Alcoutlabi, X. Zhang, Energy Environ. Sci. 4 (2011) 2682–2699.
[2] Y. Zhu, S. Murali, W. Cai, X. Li, J.W. Suk, J.R. Potts, R.S. Ruoff, Adv. Mater. 22 (2010) 3906–3924.
[3] K.S. Novoselov, A.K. Geim, S.V. Morozov, D. Jiang, Y. Zhang, S.V. Dubonos, Science 306 (2004) 666–669.
[4] G. Wang, X. Shen, J. Yao, J. Park, Carbon 47 (2009) 2049–2053.
[5] X. Zhou, F. Wang, Y. Zhu, Z. Liu, J. Mater. Chem. 21 (2011) 3353–3358.
[6] R. Liang, H. Cao, D. Qian, J. Zhang, M. Qu, J. Mater. Chem. 21 (2011) 17654–17657.
[7] G. Wang, B. Wang, X. Wang, J. Park, S. Dou, H. Ahn, K. Kim, J. Mater. Chem. 19 (2009) 8378–8384.
[8] S. Yang, X. Feng, S. Ivanovici, K. Müllen, Angew. Chem., Int. Ed. 49 (2010) 8408–8411.
[9] J.K. Lee, K.B. Smith, C.M. Hayner, H.H. Kung, Chem. Commun. 46 (2010) 2025–2027.
[10] J. Dahn, T. Zheng, L. Yinghu, J. Xue, Science 270 (1995) 590–593.
[11] K. Sato, M. Noguchi, A. Demachi, N. Oki, M. Endo, Science 264 (1994) 556–558.
[12] P. Touzain, R. Yazami, J. Maire, J. Power Sources 14 (1985) 99–104.
[13] R. Yazami, P. Touzain, Synth. Met. 12 (1985) 499–503.
[14] D.R. Dreyer, S. Park, C.W. Bielawski, R.S. Ruoff, Chem. Soc. Rev. 39 (2010) 228–240.
[15] P. Lian, X. Zhu, S. Liang, Z. Li, W. Yang, H. Wang, Electrochim. Acta 55 (2010) 3909–3914.
[16] E.J. Yoo, J. Kim, E. Hosono, H. Zhou, T. Kudo, I. Honma, Nano Lett. 8 (2008) 2277–2282.
[17] J. Hou, Y. Shao, M.W. Ellis, R.B. Moore, B. Yi, Phys. Chem. Chem. Phys. 13 (2011) 15384–15402.
[18] C. Wang, D. Li, C.O. Too, G.G. Wallace, Chem. Mater. 21 (2009) 2604–2606.
[19] W.S. Hummers, R.E. Offeman, J. Am. Chem. Soc. 80 (1958) 1339.
[20] S. Stankovich, R.D. Piner, X. Chen, N. Wu, S.T. Nguyen, R.S. Ruoff, J. Mater. Chem. 16 (2006) 155–158.
[21] J. Geng, L. Liu, S.B. Yang, S.C. Youn, D.W. Kim, J.S. Lee, J.K. Choi, H.T. Jung, J. Phys. Chem. C 114 (2010) 14433–14440.
[22] E. Peled, C. Menachem, D. Bar-Tow, A. Melman, J. Electrochem. Soc. 143 (1996) L4–L7.
[23] Z.S. Wu, W. Ren, L. Xu, F. Li, H.M. Cheng, ACS Nano 5 (2011) 5463–5471.
[24] F. Campana, H. Buqa, P. Novák, R. Kötz, H. Siegenthaler, Electrochem. Commun. 10 (2008) 1590–1593.
[25] Q. Cheng, J. Tang, J. Ma, H. Zhang, N. Shinya, L.C. Qin, Phys. Chem. Chem. Phys. 13 (2011) 17615–17624.
[26] X. Zhao, C.M. Hayner, H.H. Kung, J. Mater. Chem. 12 (2011) 17297–17303.
[27] J.T. Robinson, J.S. Burgess, C.E. Junkermeier, S.C. Badescu, T.L. Reinecke, F.K. Perkins, Nano Lett. 10 (2010) 3001–3005.
[28] H.A. Becerril, J. Mao, Z. Liu, R.M. Stoltenberg, Z. Bao, Y. Chen, ACS Nano 2 (2008) 463–470.
[29] A. Abouimrane, O.C. Compton, K. Amine, S.T. Nguyen, J. Phys. Chem. C 114 (2010) 12800–12804.
[30] M.D. Levi, E.A. Levi, D. Aurbach, J. Electroanal. Chem. 421 (1997) 89–97.
[31] C. Li, X. Yin, L. Chen, Q. Li, T. Wang, J. Phys. Chem. C 113 (2009) 13438–13442.
[32] H. Buqa, A. Würsig, J. Vetter, M. Spahr, F. Krumeich, P. Novák, J. Power Sources 153 (2006) 385–390.
[33] S.L. Chou, Y. Zhao, J.Z. Wang, Z.X. Chen, H.K. Liu, S.X. Dou, J. Phys. Chem. C 114 (2010) 15862–15867.
[34] Y.P. Wu, E. Rahm, R. Holze, J. Power Sources 114 (2003) 228–236.
[35] M.D. Levi, D. Aurbach, J. Electroanal. Chem. 421 (1997) 79–88.
[36] S.W. Lee, N. Yabuuchi, B.M. Gallant, S. Chen, B.S. Kim, P.T. Hammond, H.Y. Shao, Nat. Nanotechnol. 5 (2010) 531–537.